

## Nonequilibrium mode competition in a pumped dye-filled cavity

M. Vlaho<sup>\*</sup> and A. Eckardt<sup>†</sup>

*Institut für Theoretische Physik, Technische Universität Berlin, Hardenbergstrasse 36, 10623 Berlin, Germany*

 (Received 8 September 2021; accepted 3 December 2021; published 15 December 2021)

We consider a homogeneously pumped photon gas coupled to a dye medium and investigate how its steady state is affected when varying the pump power, the photon cavity lifetime, and the cutoff frequency. We study how the interplay between pumping, loss, and dye-induced thermalization influences the selection of the cavity modes that acquire large occupation. Depending on the parameter regime, the latter can be related either to lasing of (typically multiple) modes or to equilibrium-like photon condensation in the ground mode. We calculate and explain the phase diagram of the system, with a particular emphasis on the role played by mode competition that occurs in the regime of weak cavity loss.

DOI: [10.1103/PhysRevA.104.063709](https://doi.org/10.1103/PhysRevA.104.063709)

### I. INTRODUCTION

Following the realization of Bose-Einstein condensation (BEC) of exciton polaritons, [1–6], thermalization [7] and the formation of an equilibrium-like Bose condensate of photons has been realized in various experimental setups [8–14]. The inherently grand-canonical statistics of photon BECs [15] has been studied, as well as its spatial [16] and temporal features [17–20]. A considerable amount of work has also been done to clarify the delimitation of photon BECs from lasers [21–25], and thermo-optic imprinting has been used to create variable potentials for coupled photon condensates [26].

Given the inherently driven-dissipative nature of these systems, a complex interplay between the pump and loss processes driving the system out of equilibrium and the thermalizing influence of the environment (dye solution) emerges when tuning the various control parameters. This nonequilibrium nature of these systems makes them an excellent experimental platform for studying ordering under nonequilibrium conditions. First studies of this physics have recently been published. The case of a symmetrically pumped system and its steady-state featuring multimode condensates has been studied theoretically [27], predicting a complex phase diagram, where the phases are distinguished by their different combinations of macroscopically populated modes, as well as experimentally [13]. Multimode condensates were also shown to occur in continuously pumped systems of trapped polaritons [28,29]. The case where the system of cavity-confined photons coupled to dye molecules is driven by an off-centered pump beam has also been investigated and shown to feature a robust mechanism for controlled two-mode emission [30].

Here we consider the case of a symmetrically (homogeneously) pumped system, in which multimode condensates occur. We show how the limit of a quasiequilibrium photon BEC is approached via mode competition when the photon

cavity lifetime is increased. Moreover, we also discuss the role played by the cutoff frequency, i.e., the ground-mode energy, in the formation of multimode condensates.

This paper is organized as follows. In Sec. II we introduce the model system, described in terms of rate equations for the photon mode populations  $n_i$  and the spatially dependent fraction  $f(\vec{r})$  of excited dye molecules. Then in Sec. III we discuss the condition for mode selection, i.e., a mode acquiring macroscopic occupation. We also explain how this condition is connected to the locking of the chemical potential as a BEC condition in the equilibrium limit (Sec. IIIA). We give a general condition for the threshold pump rate for a mode selection, which reduces to very simple expression in the case of first selection (Sec. IIIB). Before turning to discuss our results, we list all the parameter values corresponding to the relevant experiments and used in the numerical simulations (Sec. IIIC). In the following section (Sec. IV), we investigate the dependence of mode selection on the so-called thermalization parameter, which is effectively a dimensionless photon cavity lifetime. Here we observe and discuss the effect of mode competition with the associated cross-saturation phenomenon, as well as deselection (loss of macroscopic occupation) [27,31], before presenting a phase diagram in a parameter plane spanned by the pump rate and the thermalization parameter (Sec. V). We explain the various phase boundaries and how the approach towards a quasiequilibrium ground-mode condensate manifests in the phase diagram. Moreover, we point out discrepancies with respect to the previously computed phase diagram of Ref. [27]. In the final section (Sec. VI) we study how the mode selection is affected when tuning the cutoff-frequency.

### II. SYSTEM AND MODEL

We describe the system in terms of semiclassical equations of motion [16,27,30,32] for the photon mode populations  $n_i$  and the fraction  $f(\vec{r})$  of excited dye molecules at position  $\vec{r}$  in

<sup>\*</sup>vlaho@tu-berlin.de

<sup>†</sup>eckardt@tu-berlin.de

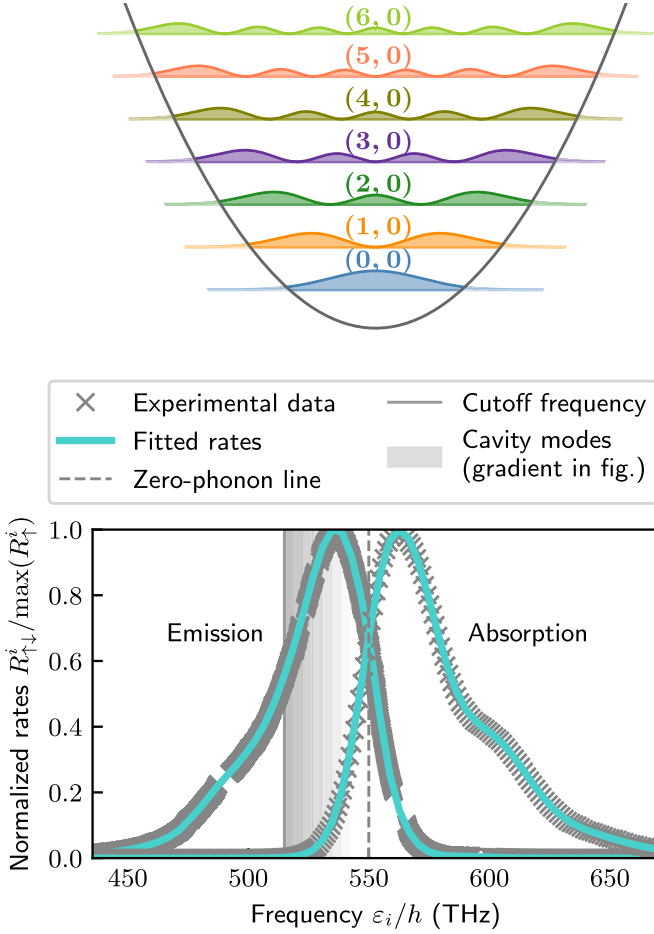


FIG. 1. Upper panel: Photon mode densities  $|\psi_{n_x, n_y}(x)|^2$  projected onto the  $x$  axis. For simplicity, only modes  $(n_x, 0)$ , with nodes only along the  $x$  direction, are shown. Lower panel: Fitted absorption ( $R_{\downarrow}^i$ ) and emission ( $R_{\uparrow}^i$ ) rates (solid lines) vs frequency  $\varepsilon_i/h$ . The rates are fitted to experimental data (crosses) [16,38] using a cubic smoothing spline. The frequency range of the relevant cavity modes is indicated by the shaded gray area with a sharp cutoff at  $\omega_c = \varepsilon_0/h$ .

the two-dimensional space given by the directions perpendicular to the optical axis of the cavity:

$$\dot{n}_i = -\kappa n_i + (n_i + 1)R_{\downarrow}^i \rho G_i - n_i R_{\uparrow}^i \rho (1 - G_i), \quad (1)$$

$$\begin{aligned} \dot{f}(\vec{r}) = & [1 - f(\vec{r})] \left( P + \sum_i R_{\uparrow}^i |\psi_i(\vec{r})|^2 n_i \right) \\ & - f(\vec{r}) \left[ \Gamma + \sum_i R_{\downarrow}^i |\psi_i(\vec{r})|^2 (n_i + 1) \right]. \quad (2) \end{aligned}$$

Here  $\rho$  is the density of the dye molecules,  $\Gamma$  is the rate of spontaneous losses into noncavity modes, and  $\kappa$  is the photon loss rate. The transverse photonic modes  $\psi_i(\vec{r})$  (upper panel of Fig. 1) are the eigenfunctions of the two-dimensional harmonic trap imposed by the spherically curved mirrors. They are characterized by a pair of harmonic oscillator quantum numbers in the  $x$  and  $y$  directions,  $i = (v_x, v_y)$ , and have energies  $E_i = \hbar[\Omega_x(v_x + 1/2) + \Omega_y(v_y + 1/2)]$  with oscillator frequencies  $\Omega_x$  and  $\Omega_y$ . In the following, we assume  $\Omega_x$  and

$\Omega_y$  to be almost identical,  $\Omega_x \equiv \Omega$  and  $\Omega_y = 0.99\Omega$ . This slight anisotropy of the trap is a realistic assumption and is required for eliminating the coherent mixing of otherwise degenerate modes  $i$  [33]. The harmonic oscillator length  $d$  associated with  $\Omega$  is used as a natural unit of length. The total energy of the cavity mode  $i$  is then given by  $\varepsilon_i = E_i + \hbar\omega_L$ , where  $\omega_L$  is the frequency of the relevant longitudinal mode. The gain [34] of mode  $i$  is quantified by its overlap with the fraction  $f(\vec{r})$  of excited dye molecules,

$$G_i[f(\vec{r})] = \int |\psi_i(\vec{r})|^2 f(\vec{r}) d\vec{r} \in [0, 1]. \quad (3)$$

The dye solution is characterized by the absorption and emission rates,  $R_{\uparrow}^i$  and  $R_{\downarrow}^i$ , which satisfy the Kennard-Stepanov law [7,35,36]

$$R_{\downarrow}^i/R_{\uparrow}^i = C e^{-\beta(\varepsilon_i - \hbar\omega_z)}, \quad (4)$$

which can enable the photon gas to thermalize. Here  $\omega_z$  denotes the zero-phonon frequency of the dye and  $C$  is a frequency-independent proportionality constant. The pump rate  $P$  is considered to be spatially constant [37].

### III. MODE SELECTION

We can write the steady state of Eq. (1) in the following form:

$$n_i = \left( \frac{R_{\uparrow}^i (1 - G_i)}{R_{\downarrow}^i G_i} - 1 + \frac{\kappa}{R_{\downarrow}^i \rho G_i} \right)^{-1}. \quad (5)$$

When a mode  $i$  becomes macroscopically occupied (“Bose selected” [23,24,39,40]), the contribution of spontaneous emission to this macroscopic population  $n_i$  becomes negligible ( $n_i + 1 \approx n_i$ ). This allows us to find a sharply defined threshold value  $G_i^{th}$  of the gain at which the “selection” happens. It is obtained by setting the term in the brackets to zero (corresponding to a divergent occupation). We get

$$G_i^{th} = \frac{R_{\uparrow}^i + \kappa/\rho}{R_{\uparrow}^i + R_{\downarrow}^i} = \frac{1 + R_{\uparrow}^0/(R_{\uparrow}^i \xi)}{1 + C e^{-\beta(\varepsilon_i - \hbar\omega_z)}}, \quad (6)$$

where we have isolated the thermalization parameter [16,27]

$$\xi = R_{\uparrow}^0 \rho / \kappa \quad (7)$$

as a dimensionless measure of the coupling between the photons and the dye relative to the cavity loss. Since one of the requirements of an effective thermalization in the system is that the absorption at the ground mode is not too low,  $R_{\uparrow}^0$  is a reasonable choice in this definition. However, it is somewhat arbitrary, and it does not affect the results, given that the same quantity is divided from the absorption and emission rates  $R_{\uparrow, \downarrow}^i$  to obtain the dimensionless form of the rate equations used in the numerical calculations. Once a mode is selected, the gain  $G_i$  is clamped [41] close to (i.e., slightly below) the threshold value  $G_i^{th}$ .

#### A. Equilibrium limit

In the case of equilibrium BEC, this “divergent” (macroscopic) occupation in the ground mode happens when the chemical potential approaches the value of ground mode energy. This locking of the chemical potential can be shown

to be equivalent to the above defined clamping of the gain  $G_i$  in the limit  $\xi \rightarrow \infty$  for the case of homogeneous excitation field  $f(\vec{r}) = \text{const} \equiv f$ . Equation (5) then reduces to the Bose-Einstein distribution

$$n_i = (e^{\beta(\varepsilon_i - \mu)} - 1)^{-1}, \quad (8)$$

where we have used the Kennard-Stepanov law [Eq. (4)] and introduced the chemical potential  $\mu$  of the photon gas given by [42]

$$e^{\beta\mu} = C e^{\beta\hbar\omega_c} f / (1 - f), \quad (9)$$

where  $f/(1-f)$  is now a spatially homogeneous ratio of the number of excited and ground-state dye molecules. When  $\mu \rightarrow \varepsilon_0$  (onset of BEC), Eq. (9) becomes  $C e^{-\beta(\varepsilon_0 - \hbar\omega_c)} = (1 - f)/f$ . It follows that  $f = G_0^{th} = 1/(1 + C e^{-\beta(\varepsilon_0 - \hbar\omega_c)})$ , which is exactly the selection threshold condition for the ground mode given by Eq. (6) when the photon cavity lifetime  $1/\kappa \propto \xi \rightarrow \infty$ . Therefore, in the equilibrium limit, which does not require pumping in order to stabilize the average photon number, the locking of the chemical potential is equivalent to the clamping of the gain.

### B. Threshold pump rate

The general condition for the selection threshold pump rate  $P_i^{th}$  of mode  $i$  can be obtained by inserting Eq. (2) into the definition of the gain (3) and setting it equal to  $G_i^{th}$ . We get [27]

$$G_i^{th} = \int d\vec{r} |\psi_i(\vec{r})|^2 \frac{P + \sum_{j \in S} R_{\uparrow}^j |\psi_j(\vec{r})|^2 n_j}{\Gamma + P + \sum_{j \in S} (R_{\uparrow}^j + R_{\downarrow}^j) |\psi_j(\vec{r})|^2 n_j}, \quad (10)$$

where the sums in the integrand are over all of the modes which have already been Bose selected at lower pump rates. Again, the sharpness of transitions allows us to omit the contributions of spontaneous emission to the mean occupations, which are negligible once a mode is selected.

This equation would allow us, in principle, to iteratively determine each selected mode and the corresponding threshold pump rate, if the populations of all the already selected modes are known as a function of the pump rate  $P$ . Namely, at each value of  $\xi$ , the selected mode is the one for which Eq. (10) holds for the lowest value of  $P$ . However, an analytic expression can be obtained only for the first selection. Here the approximate value of the threshold  $P_i^{th}$  can be obtained by setting all  $n_j$  to zero (i.e., neglecting the coupling to the still weakly occupied photonic modes). Equation (10) then reduces to

$$G_i^{th} = \frac{P}{\Gamma + P}. \quad (11)$$

Solving this equation for  $P$  and inserting the condition (6), we get the first-selection threshold pump rate  $P_i^{th}$  as a function of the thermalization parameter  $\xi$ :

$$P_i^{th} = \frac{G_i^{th}}{1 - G_i^{th}} \Gamma = \frac{R_{\uparrow}^i + R_{\uparrow}^0/\xi}{R_{\downarrow}^i - R_{\downarrow}^0/\xi} \Gamma. \quad (12)$$

It follows that the first-selected mode is the one with the lowest threshold gain  $G_i^{th}(\xi)$ . In Fig. 2 the threshold pump rate  $P_i^{th}$  is shown as a function of  $\xi$  and the mode energy

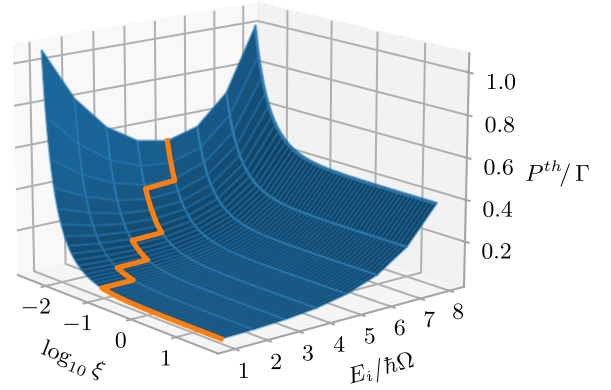


FIG. 2. Threshold pump rate  $P_i^{th}$  of the first selection as a function of the thermalization parameter  $\xi$  and the energy  $E_i$  of the modes.

$E_i$  [blue (dark gray) surface]. The orange (light gray) line on this surface follows the minimal  $P_i^{th}$  at each value of  $\xi$ . We see that only for very small values of the thermalization parameter,  $\xi \lesssim 0.1$ , this is not the ground mode. This follows from Eq. (6) when taking into account the shapes of the absorption and emission spectra (see the lower panel of Fig. 1). In particular, by looking at the second equation we see that the  $\xi$ -independent denominator always favors the ground mode, which has the largest Boltzmann factor, whereas the nominator contains the relative absorption rate of mode  $i$ ,  $R_{\uparrow}^i/R_{\uparrow}^0$ , modulated by the thermalization parameter. When the latter is sufficiently large,  $\xi \gtrsim 0.1$ , this term becomes negligible compared to 1, and the selected mode is determined solely by the ground-mode favoring Boltzmann factor. On the other hand, in the high loss regime,  $\xi \lesssim 0.1$ , excited modes with higher relative absorption rate can “win out,” i.e., have the smallest threshold gain.

### C. System parameters

For our numerical calculation we use the parameter values which correspond to the experiments of Refs. [21,26], namely, we choose a slightly anisotropic harmonic trap, as defined above, with  $\Omega/2\pi = 4$  THz. The ground-mode (cut-off) frequency is set to  $\omega_c = \varepsilon_0/\hbar = 2\pi \times 515$  THz. From the measured absorption and fluorescence spectra of the Rhodamine 6G dye [16], we obtain the corresponding rates  $R_{\uparrow,\downarrow}^i$  as fitted functions of the frequency  $\varepsilon_i/\hbar$  [16,38] using a cubic smoothing spline, as shown in the lower panel of Fig. 1. The values of the absorption and emission rates across the whole frequency range are then determined by setting the absorption rate of the ground mode to  $R_{\uparrow}^0/d^2 = 1$  kHz [21]. The density of dye molecules is set to  $\rho = 10^8/d^2$ , and the thermalization parameter  $\xi$  lies between 0.01 and 100, where  $\xi = 25$  corresponds to the mean experimental value of the photon loss rate  $\kappa \approx 4$  GHz [21]. The rate of spontaneous losses into noncavity modes is set to  $\Gamma = 0.2$  GHz.

We kept 28 modes (corresponding to seven energy levels) in our numerical calculations. The value of the frequency spacing  $\Omega$  between the modes was chosen large enough, while also achievable experimentally [26], so that increasing the number of modes considered would not produce a

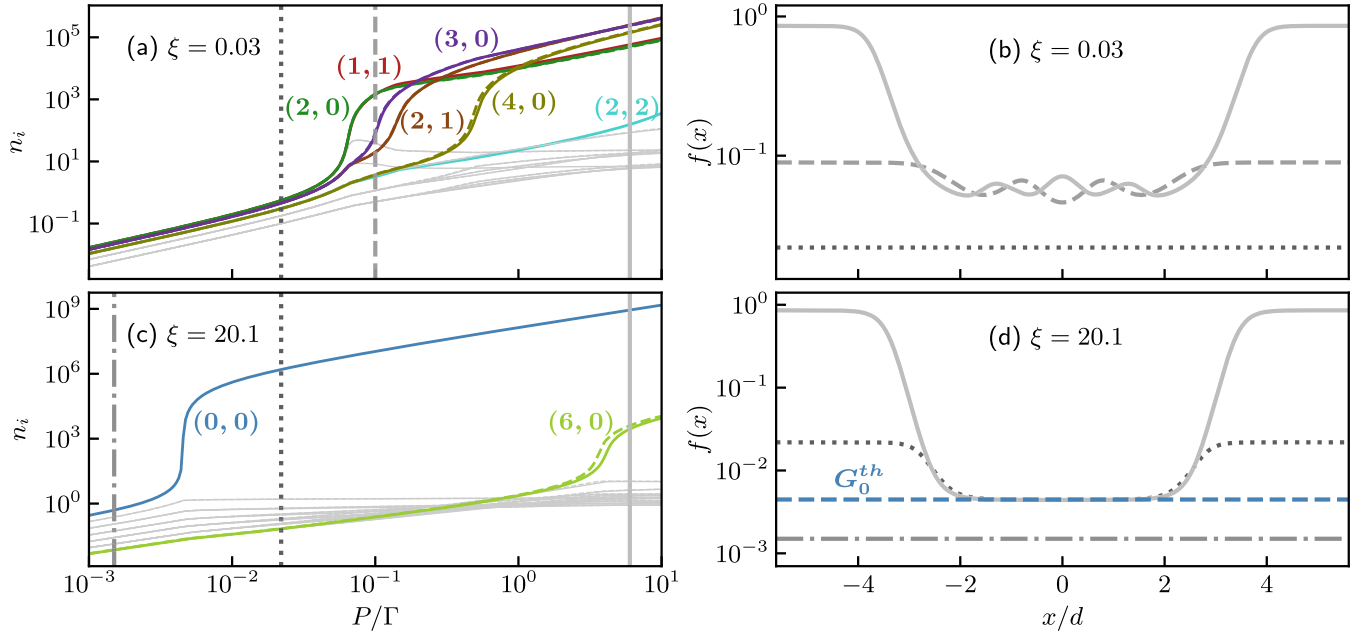


FIG. 3. The left panel shows the mode populations  $n_i$  as functions of pump rate  $P$  for two values of the thermalization parameter,  $\xi = 0.03$  (a) and  $\xi = 20.1$  (c). Only one of the modes in an almost identically behaving symmetric pair is labeled. The right panel, (b) and (d), shows the corresponding spatial distributions of excited dye molecules  $f(x)$  for the chosen values of  $P$  (vertical lines in the left panel).

significant effect on the results. That is, any additional modes would remain unselected across the whole pump-rate range and would not affect the transition thresholds of the selected modes. We used the LSODA algorithm and set a sufficiently large time interval to achieve convergence to a steady state for the range of parameters used. The initial condition was set to a zero mode-population vector for the lowest value in a range of pump rates  $P$ , and adapted to the current solution at each successive value of  $P$ . We also solved the steady-state equation directly via a root-finding algorithm to confirm that both methods produce exactly the same results.

#### IV. TUNING THE PHOTON CAVITY LIFETIME AND MODE COMPETITION

Let us now discuss how the selection of modes is influenced by the thermalization parameter  $\xi$ , or equivalently the photon cavity lifetime  $1/\kappa$ . Numerically obtained photon mode populations as functions of the pump rate are shown in Fig. 3 for two values of the thermalization parameter  $\xi$ . The colors correspond to the modes as shown in Fig. 1, and only modes with varying shapes are shown with different colors; e.g., symmetric pairs like  $(2,1)$  and  $(1,2)$  are depicted with the same color [brown (dark gray)] but a different line style (solid vs dashed). These same colors are used consistently in all figures in this paper. As expected from Fig. 2, for the low value  $\xi = 0.03$  [Fig. 3(a)], multiple quasidegenerate excited modes  $(2,0)$ ,  $(0,2)$ , and  $(1,1)$  are selected at practically identical threshold pump rate. This is followed by further selection of modes with higher energy, while the ground mode  $(0,0)$  remains unselected.

When  $\xi$  is sufficiently large, as shown in Fig. 3(c), the ground mode is the first one to get selected at a much lower value of  $P$ . However, as  $P$  is increased further, eventually

also modes  $(6,0)$  and  $(0,6)$  get selected, as opposed to the energetically favorable selection of the first excited modes  $(1,0)$  and  $(0,1)$ , which according to Eq. (6) possess a lower threshold gain  $G_i^{th}$ .

In order to explain this, we plot the fraction of excited dye molecules  $f(x) \equiv f(x, 0)$  in Fig. 3(d) for three chosen values of  $P$  (indicated by vertical lines of the same style in the left panel). We see that once  $P$  is increased above the first selection threshold, the shape of  $f(x)$  reflects the clamping of the gain in the central region, which overlaps with the selected ground-state mode. This clamping in the center of the trap then suppresses the selection of further low-energy modes, whose wave functions have a large weight in the trap center. This mechanism of cross-saturation [43–45] explains why after the ground mode, the next modes to be selected possess six excitation quanta. Likewise, Fig. 3(b) shows that after the first selection  $f(x)$  reflects the shape of the selected excited modes for the scenario of Fig. 3(a).

To see more clearly how the shape of  $f(x)$  and with that the cross-saturation effect changes with  $\xi$ , we plot its value at  $P = 0.02$  for 4 values of  $\xi$  (Fig. 4). This pump rate is slightly above the first selection threshold  $P^{th}$ , and only the ground mode is selected in each case. It follows from Eqs. (6) and (12) that a higher value of  $\xi$  lowers the first selection threshold, and the corresponding gain gets clamped at a lower value  $G_0^{th}$ , indicated by horizontal blue (gray) lines for each  $\xi$  in Fig. 4. We see that with an increase of  $\xi$  the excited dye molecules are clamped both at a lower value and in a wider spatial region, therefore becoming progressively more inaccessible to modes close in energy to the ground mode. In other words, when the gain is clamped at lower values, not enough molecules can be excited in the region of overlap between the ground mode and following excited modes. We can say that successive modes (those with largest overlap) “compete” for gain in the

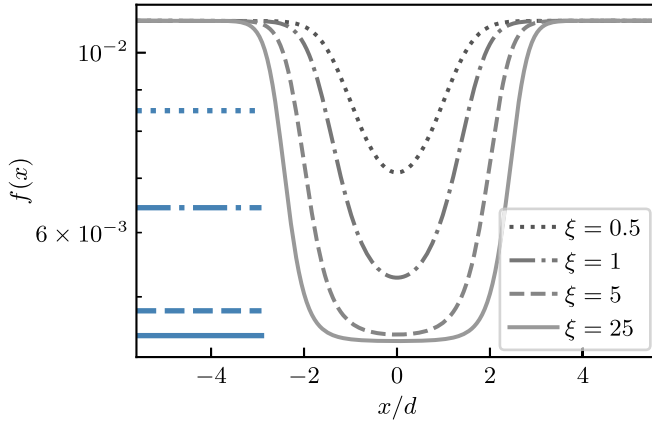


FIG. 4. Spatial distributions of excited dye molecules  $f(x)$  close above the first selection threshold  $P^{th}$  for four values of the thermalization parameter  $\xi$ . The corresponding threshold gain  $G^{th}$  is marked by a horizontal blue (gray) line of the same style.

same spatial domain and block each other from being selected together in the regime of higher  $P$ . When the thermalization parameter is increased even further to  $\xi = 20.1$  [Fig. 3(d)]  $f(x)$  is locked to an even lower threshold value of the gain  $G_0^{th}$  [dashed blue (gray) line] in an even wider middle region. In this way, when increasing  $\xi$ , a quasiequilibrium steady state is approached, where the gain clamping is equivalent to locking of the chemical potential. The fact that  $f(x)$  is free to increase with the pump power in the outer spatial region until gain saturation is reached (no more dye molecules available to excite) reflects the nonequilibrium nature of the system.

Another observation that we can make from Fig. 3 is that, while the modes (6,0) and (0,6) are selected in high  $P$  regime, all the other modes with the *same* energy [like (3,3), (4,2), (5,1), etc.] remain unselected due to the key influence of the dye excitation profile on the behavior of modes. This is another indicator of the nonequilibrium nature of this state [even though at lower  $P$  where only (0,0) is selected, this state can hardly be distinguished from the equilibrium photon BEC (of a finite system), as will be discussed below in more detail].

In Fig. 5, at an intermediate value of the thermalization parameter  $\xi = 1.8$ , we can also observe the phenomenon of “deselection.” Namely, we can see that the green (gray)-colored mode pair (2,0) and (0,2) gets deselected, as the purple (dark gray)-colored one (3,0) and (0,3) is selected [Fig. 5(a)] [henceforth for brevity, mode pairs  $\{(i, j), (j, i), i \neq j\}$  are denoted simply as “mode pair  $(i, j)$ ”]. This decondensation of photonic modes was already discussed in Ref. [27], and a similar effect was predicted in a system of driven-dissipative polariton condensate [31]. This is another manifestation of the above-mentioned competition between successive modes which have a large spatial overlap. It happens when not enough dye molecules are pumped to their excited states in the combined region of mode density for both mode pairs to stay selected. Once, after the ground mode, the mode pair (2,0) is selected,  $f(\vec{r})$  can increase only in a very restricted way, such that it stays clamped close to both  $G_{(0,0)}$  and  $G_{(2,0)}$  [dotted lines in Fig. 5(c)]. This restriction still allows for the selection of the mode pair (3,0). However, the more particles this third selected pair acquires, the more attractive it becomes

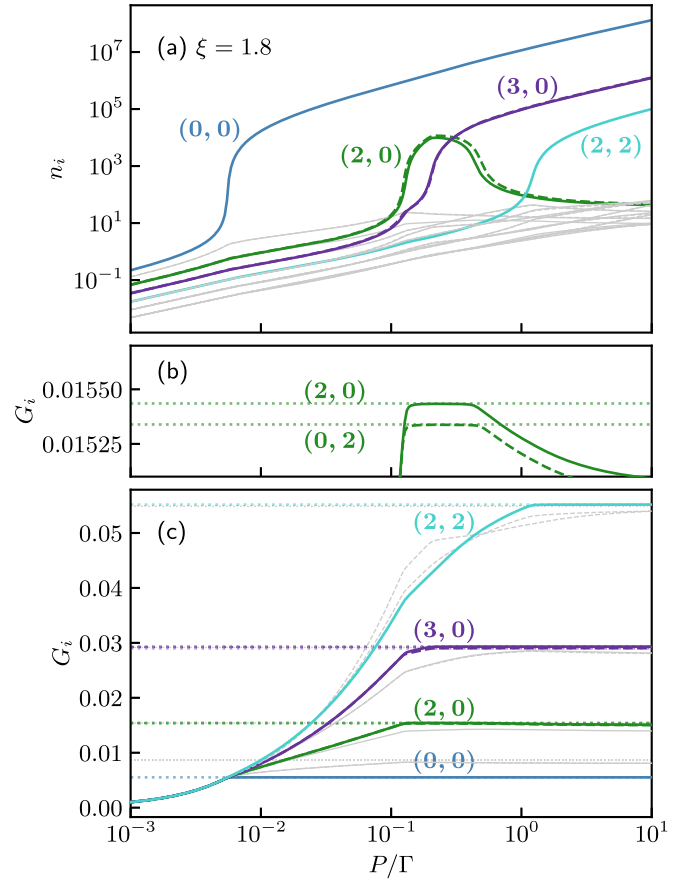


FIG. 5. Population  $n_i$  (a) and gain  $G_i$  (c) of modes  $i$  vs pump rate  $P$  for  $\xi = 1.8$ . Only one of the modes in an almost identically behaving symmetric pair is labeled. Dotted horizontal lines indicate threshold values  $G_i^{th}$  to which the gain is clamped at selection. The middle panel (b) shows the zoomed-in gain of modes (2,0) and (0,2), which are deselected when the clamped gain starts to drop below  $G_{(2,0)}^{th}$  and  $G_{(0,2)}^{th}$ , respectively.

for further photons due to bosonic enhancement (i.e., stimulated emission). This nonlinear effect leads to a competition with the energetically slightly favored (2,0) modes, which eventually causes the decondensation of the latter. This is accompanied by the “declamping” of its gain, which is better visible in Fig. 5(b) showing the zoom-in around  $G_{(2,0)}^{th}$ .

## V. PHASE DIAGRAM

After having discussed the role of mode competition for the selection of excited cavity modes, let us now compute the phase diagram of the system in the parameter plane spanned by the pump rate and the thermalization parameter. Figure 6 shows a phase diagram where the various phases are characterized by which modes are selected. There are no macroscopically occupied modes in the white region (labeled 1). Only the ground mode is selected in the blue region (2), whereas in the gray one (3), there are multiple selected modes. Dots (crosses) are numerical points indicating selections (deselections) of the corresponding modes. The lower and upper phase boundaries (dotted lines) are obtained by interpolating between the points of first (second) selection. Below the value

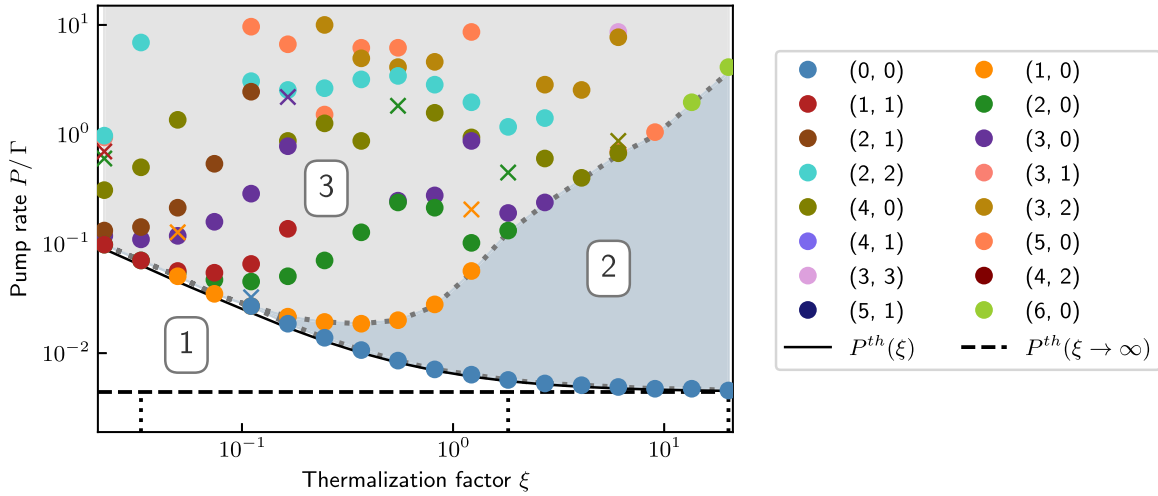


FIG. 6. Phase diagram showing three main regions. The white region (labeled 1) has no selected modes, only the ground mode is selected in the blue region (2), and there are multiple selections in the gray one (3). Dots (crosses) are numerical points indicating selections (deselections) of the corresponding modes. The dotted line is the lower (upper) phase boundary, interpolating between the points of first (second) selection. The pump rate at which the two phase boundaries meet is the minimal  $P$  for which the ground mode is selected. Below this pump rate (“lasing phase”), the phase boundaries are indistinguishable, because multiple quasidegenerate higher energy modes are selected at almost exactly the same  $P$ . The analytical result for the first selection threshold [Eq. (12)] is shown with a solid black line. In the high- $\xi$  regime, this phase boundary approaches the dashed horizontal line, showing the high thermalization limit of Eq. (12)  $P^{th}(\xi \rightarrow \infty)$ . The three dotted vertical lines mark the cuts through the phase diagram shown in Fig. 3 and Fig. 5.

of  $\xi$  at which both boundaries meet, the mode which becomes selected first is not the ground state anymore. Below this point, the two phase boundaries are indistinguishable, because multiple quasidegenerate higher energy modes are selected at almost exactly the same  $P$ . The solid black curve indicates the analytical result for the first selection threshold, given by Eq. (12) and shown with the orange (light gray) line in Fig. 2. It closely matches the numerical result, especially in the high  $\xi$  regime, where it approaches the high thermalization limit of Eq. (12)  $P^{th}(\xi \rightarrow \infty)/\Gamma = R_{\uparrow}^0/R_{\downarrow}^0$  (dashed horizontal line).

We note that our phase diagram differs from the one obtained in Ref. [27]. Namely, in agreement with the analytical prediction (12), we find that the threshold pump rate for the first selection process decreases as a function of the thermalization parameter, while it increases in Ref [27].

In the regime of low  $\xi$ , where the photon cavity lifetime is too short for photons to effectively thermalize, there are multiple high-energy modes selected closely together instead of the ground mode, and these transitions to macroscopic occupation represent the limit where the operation of the system would typically be considered as that of a laser. Given that drive and thermalization are both present in this system, Bose condensation cannot be sharply distinguished from lasing. Nevertheless, this phase diagram still clearly shows the trend of going from the lasing limit towards the BEC limit as the thermalization parameter is ramped up.

The second phase boundary separates the blue region (2) with only the ground state selected from the gray one (3), where also excited modes have acquired a large occupation. With increasing  $\xi$ , the separation between the  $P_0^{th}$  of the ground mode selection and the  $P_j^{th}$  of the next selected mode  $j$  increases together with its energy  $E_j$ , due to mode competition explained above. In this way, a limit of quasiequilibrium

photon BEC is approached for large  $\xi$  and pump powers well below the second selection threshold.

To support this claim, in Fig. 7 we compare the Bose-Einstein (BE) distribution  $\ln(1 + 1/n_i) = \beta\varepsilon_i - \mu$  [solid orange (light gray) line] with the distribution of numerically obtained mode populations  $n_i$  [blue (gray) dots] for  $P$  close and far above the first selection threshold  $P^{th}$ . Left panel

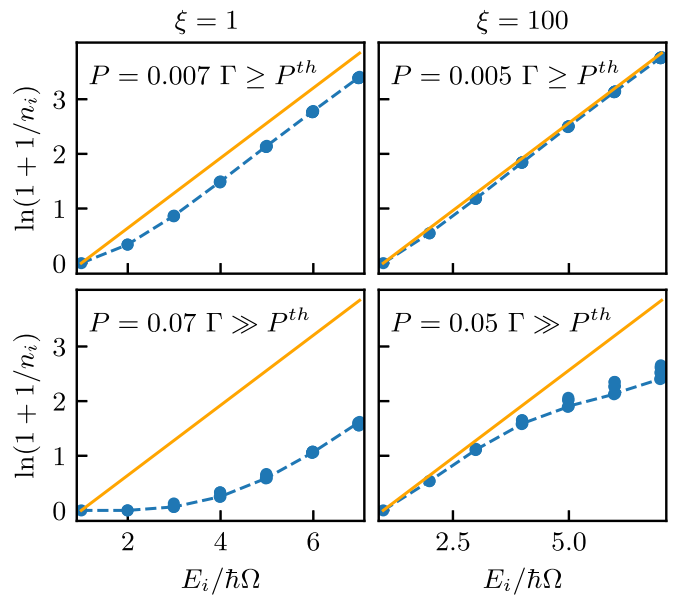


FIG. 7. Numerical mode population  $n_i$  [blue (gray) dots] vs mode energy  $E_i$  compared to the thermal distribution [solid orange (light gray) line] below, close above and far above the first selection threshold  $P^{th}$  when  $\xi = 1 \Rightarrow P^{th} = 0.0065 \Gamma$  (left panels) and  $\xi = 100 \Rightarrow P^{th} = 0.0044 \Gamma$  (right panels).

corresponds to  $\xi = 1$ , and the right one to  $\xi = 100$ , for which only the ground mode is selected. As expected, for higher  $\xi$ , the match between the numerical points and the thermal distribution is better, particularly when  $P$  is only slightly above the threshold,  $P \gtrsim P^{th}$ . Here the small deviations are only due to the fact that the absorption and emission rates fitted to measured data (Fig. 1) do not satisfy the Kennard-Stepanov relation [Eq. (4)] exactly, but only to a very good approximation. As  $P$  is raised significantly above  $P^{th}$ , the numerically obtained populations start to deviate from the BE distribution, particularly those of higher modes. This is expected, even though at the very high value of  $\xi$ , no other mode is selected at  $P \gg P^{th}$  except the ground mode. The reason for this is that outside of the increasingly wide central region of the trap where the gain is clamped,  $f(x)$  can still increase with  $P$ . Therefore, the occupation of modes with a high density there (higher energy modes) can increase as well, moving away from the thermal distribution.

## VI. TUNING THE CUTOFF FREQUENCY

Let us finally discuss how the physics of the mode selection changes, when considering a variation of the cutoff frequency  $\omega_c$  (or, equivalently, the detuning from the zero-phonon line). The cutoff frequency corresponds to the ground-mode energy and can be tuned experimentally by varying the longitudinal frequency  $\omega_L$  via the cavity length. It determines the absorption and emission rates, thus affecting also the degree of thermalization. This has been studied experimentally for the case of a continuous wave (CW) [7] and pulsed laser pump [21], as well as in theoretical work [17].

In Fig. 8 we show the numerical results for the photon populations  $n_i$  for three different values of the cutoff frequency, while keeping the thermalization parameter fixed at  $\xi = 1$ . Changing the cutoff frequency, i.e., the ground-mode energy, corresponds to shifting the frequency range of cavity modes (sketched by the gray shaded area in the lower panel of Fig. 1) to the left or right. This effects the threshold gain  $G_i^{th}$  of each mode [Eq. (6)]. For sufficiently low cutoff frequency  $\omega_c/2\pi = 490$  THz [Fig. 8(a)], the tabulated values for the absorption and emission rates no longer satisfy the Kennard-Stepanov law. Instead of the ground mode, now an excited mode pair (3,0) has the lowest value of  $G_i^{th}$  and it is selected first, closely followed by additional excited modes, while the ground mode remains unselected. In the case of higher  $\omega_c/2\pi = 515$  THz (the same value is used for all the rest of our results), the ground mode is selected first, followed by the selection of several excited modes, as seen in Fig. 8(b). Compared to Fig. 8(a), the threshold pump rate  $P^{th}$  of the first selection has increased. When the cutoff frequency is shifted even further to  $\omega_c/2\pi = 525$  THz, only the ground mode is selected before the gain is saturated [Fig. 8(c)] and no further selections can occur. This is shown in the inset, where the  $P$  axis is extended by two orders of magnitude. In this case the Kennard-Stepanov law still holds, but the corresponding  $P^{th}$  and  $G^{th}$  are now the highest. It should be pointed out that in the actual experiment, as the cutoff frequency is varied, the photon cavity lifetime also varies significantly [21]. In the case of our chosen  $\omega_c$  values, this means that  $\xi$  should increase with  $\omega_c$  [46]. However, this would only enhance the

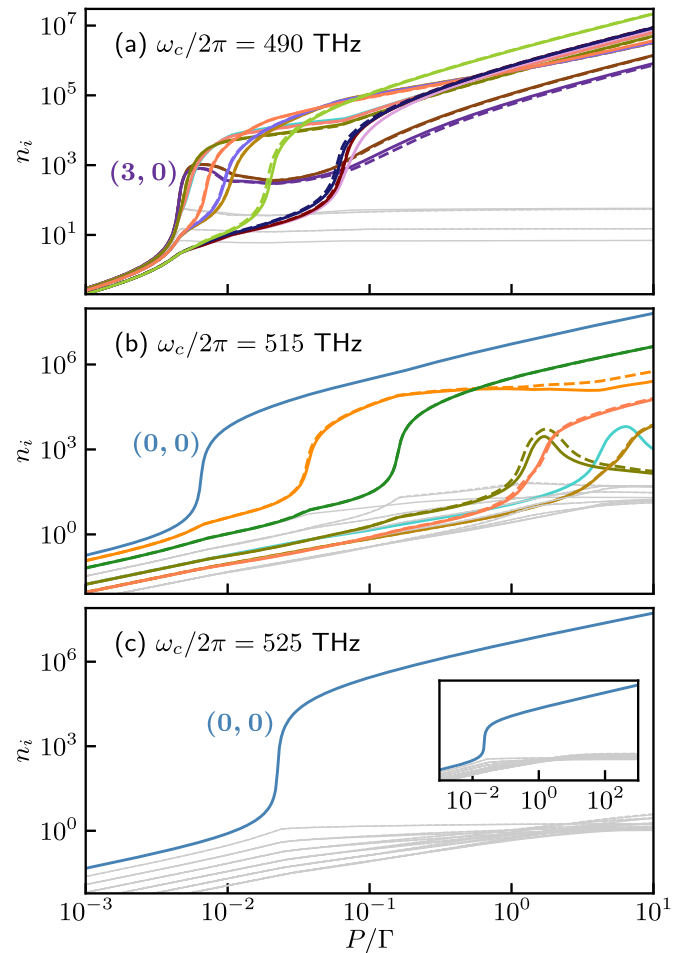


FIG. 8. Population  $n_i$  of modes  $i$  vs pump rate  $P$  for  $\xi = 1$ . The cutoff frequency is  $\omega_c/2\pi = 490$  THz (a),  $\omega_c/2\pi = 515$  THz (b) and  $\omega_c/2\pi = 525$  THz (c). The inset of panel (c) contains the same result extended to high  $P$  regime, showing that only the ground mode is selected before the gain is saturated.

effect of increase in photon thermalization, observed from Figs. 8(a)–(c).

## VII. CONCLUSIONS

We have studied how the variation of the photon cavity lifetime  $1/\kappa$  and the cutoff frequency  $\omega_c$  effects the steady state of a homogeneously pumped photon gas coupled to a dye medium. We have shown how, through the effect of mode competition (governed by the dye excitation profiles), the equilibrium-like ground-mode condensation emerges from the steady state of the system. Namely, we found that increasing the thermalization parameter  $\xi \propto 1/\kappa$  results in an increased competition of transverse modes for the gain, in the sense that the ground-mode selection is followed by a selection of modes with increasing number of excitation quanta. This is explained as a consequence of how the dye excitation profile  $f(\vec{r})$  at pump powers above which the ground-mode is selected changes with  $\xi$ . We produced a phase diagram of the system in the space of two parameters, the pump power and the thermalization parameter, and noted how it differs from the one in Ref. [27].

We also looked at the effect of varying cutoff frequency  $\omega_c$  on the selection of modes, and found that, in agreement with previous work [7,17,21], below a certain value of  $\omega_c$ , the photons are unable to effectively thermalize, resulting in the closely spaced selections of many excited modes, as opposed to the ground mode. On the other hand, the cutoff frequency can be increased above the value used in the rest of this work, while keeping the ratio of emission and absorption rates still to a good approximation proportional to the Boltzmann factor

(i.e., the Kennard-Stepanov law still holds). We show that in this case only the ground mode is selected before the gain saturates.

#### ACKNOWLEDGMENTS

We acknowledge the support from the German Research Foundation (DFG) via the Research Unit FOR 2414 (Project No. 277974659).

- 
- [1] H. Deng, G. Weihs, C. Santori, J. Bloch, and Y. Yamamoto, Condensation of semiconductor microcavity exciton polaritons, *Science* **298**, 199 (2002).
- [2] J. Kasprzak, M. Richard, S. Kundermann, A. Baas, P. Jeambrun, J. M. J. Keeling, F. M. Marchetti, M. H. Szymanska, R. Andre, J. L. Staehli, V. Savona, P. B. Littlewood, B. Deveaud, and L. S. Dang, Bose-Einstein condensation of exciton polaritons, *Nature (London)* **443**, 409 (2006).
- [3] T. Byrnes, N. Y. Kim, and Y. Yamamoto, Exciton-polariton condensates, *Nat. Phys.* **10**, 803 (2014).
- [4] R. Balili, V. Hartwell, D. Snoke, L. Pfeiffer, and K. West, Bose-Einstein condensation of microcavity polaritons in a trap, *Science* **316**, 1007 (2007).
- [5] J. D. Plumhof, T. Stöferle, L. Mai, U. Scherf, and R. F. Mahrt, Room-temperature Bose-Einstein condensation of cavity exciton-polaritons in a polymer, *Nat. Mater.* **13**, 247 (2014).
- [6] Y. Sun, P. Wen, Y. Yoon, G. Liu, M. Steger, L. N. Pfeiffer, K. West, D. W. Snoke, and K. A. Nelson, Bose-Einstein Condensation of Long-Lifetime Polaritons in Thermal Equilibrium, *Phys. Rev. Lett.* **118**, 016602 (2017).
- [7] J. Klaers, F. Vewinger, and M. Weitz, Thermalization of a two-dimensional photonic gas in a ‘white wall’ photon box, *Nat. Phys.* **6**, 512 (2010).
- [8] J. Klaers, J. Schmitt, F. Vewinger, and M. Weitz, Bose-Einstein condensation of photons in an optical microcavity, *Nature (London)* **468**, 545 (2010).
- [9] J. Marelic and R. A. Nyman, Experimental evidence for inhomogeneous pumping and energy-dependent effects in photon Bose-Einstein condensation, *Phys. Rev. A* **91**, 033813 (2015).
- [10] R. Weill, A. Bekker, B. Levit, and B. Fischer, Bose-Einstein condensation of photons in an erbium-ytterbium co-doped fiber cavity, *Nat. Commun.* **10**, 747 (2019).
- [11] R. Rajan, P. Ramesh Babu, and K. Senthilnathan, Photon condensation: A new paradigm for Bose-Einstein condensation, *Front. Phys.* **11**, 110502 (2016).
- [12] R. A. Nyman and B. T. Walker, Bose-Einstein condensation of photons from the thermodynamic limit to small photon numbers, *J. Mod. Opt.* **65**, 754 (2018).
- [13] B. T. Walker, L. C. Flatten, H. J. Hesten, F. Mintert, D. Hunger, A. A. P. Trichet, J. M. Smith, and R. A. Nyman, Driven-dissipative non-equilibrium Bose-Einstein condensation of less than ten photons, *Nat. Phys.* **14**, 1173 (2018).
- [14] J. Marelic, L. F. Zajiczek, H. J. Hesten, K. H. Leung, E. Y. X. Ong, F. Mintert, and R. A. Nyman, Spatiotemporal coherence of non-equilibrium multimode photon condensates, *New J. Phys.* **18**, 103012 (2016).
- [15] J. Schmitt, T. Damm, D. Dung, F. Vewinger, J. Klaers, and M. Weitz, Observation of Grand-Canonical Number Statistics in a Photon Bose-Einstein Condensate, *Phys. Rev. Lett.* **112**, 030401 (2014).
- [16] J. Keeling and P. Kirton, Spatial dynamics, thermalization, and gain clamping in a photon condensate, *Phys. Rev. A* **93**, 013829 (2016).
- [17] P. Kirton and J. Keeling, Thermalization and breakdown of thermalization in photon condensates, *Phys. Rev. A* **91**, 033826 (2015).
- [18] B. T. Walker, H. J. Hesten, R. A. Nyman, and F. Mintert, Collective excitation profiles and the dynamics of photonic condensates, *Phys. Rev. A* **100**, 053828 (2019).
- [19] B. T. Walker, H. J. Hesten, H. S. Dhar, R. A. Nyman, and F. Mintert, Non-Critical Slowing Down of Photonic Condensation, *Phys. Rev. Lett.* **123**, 203602 (2019).
- [20] J. Schmitt, Dynamics and correlations of a Bose-Einstein condensate of photons, *J. Phys. B: At. Mol. Opt. Phys.* **51**, 173001 (2018).
- [21] J. Schmitt, T. Damm, D. Dung, F. Vewinger, J. Klaers, and M. Weitz, Thermalization kinetics of light: From laser dynamics to equilibrium condensation of photons, *Phys. Rev. A* **92**, 011602(R) (2015).
- [22] J. Schmitt, T. Damm, D. Dung, F. Vewinger, J. Klaers, and M. Weitz, Bose-Einstein condensation of photons versus lasing and Hanbury Brown-Twiss measurements with a condensate of light, *Laser Spectroscopy XXII International Conference on Laser Spectroscopy (ICOLS2015)* (World Scientific, 2017), pp. 85–96.
- [23] H. A. M. Leymann, D. Vorberg, T. Lettau, C. Hopfmann, C. Schneider, M. Kamp, S. Höfling, R. Ketzmerick, J. Wiersig, S. Reitzenstein, and A. Eckardt, Pump-Power-Driven Mode Switching in a Microcavity Device and its Relation to Bose-Einstein Condensation, *Phys. Rev. X* **7**, 021045 (2017).
- [24] D. Vorberg, R. Ketzmerick, and A. Eckardt, Unified theory for excited-state, fragmented, and equilibriumlike Bose condensation in pumped photonic many-body systems, *Phys. Rev. A* **97**, 063621 (2018).
- [25] M. Radonjić, W. Kopylov, A. Balaž, and A. Pelster, Interplay of coherent and dissipative dynamics in condensates of light, *New J. Phys.* **20**, 055014 (2018).
- [26] D. Dung, C. Kurtscheid, T. Damm, J. Schmitt, F. Vewinger, M. Weitz, and J. Klaers, Variable potentials for thermalized light and coupled condensates, *Nat. Photonics* **11**, 565 (2017).
- [27] H. J. Hesten, R. A. Nyman, and F. Mintert, Decondensation in Nonequilibrium Photonic Condensates: When Less is More, *Phys. Rev. Lett.* **120**, 040601 (2018).
- [28] P. R. Eastham, Mode locking and mode competition in a nonequilibrium solid-state condensate, *Phys. Rev. B* **78**, 035319 (2008).

- [29] J. D. Töpfer, H. Sigurdsson, S. Alyatkin, and P. G. Lagoudakis, Lotka-Volterra population dynamics in coherent and tunable oscillators of trapped polariton condensates, *Phys. Rev. B* **102**, 195428 (2020).
- [30] M. Vlaho, H. A. M. Leymann, D. Vorberg, and A. Eckardt, Controlled two-mode emission from the interplay of driving and thermalization in a dye-filled photonic cavity, *Phys. Rev. Research* **1**, 033191 (2019).
- [31] H. Sigurdsson, I. A. Shelykh, and T. C. H. Liew, Switching waves in multilevel incoherently driven polariton condensates, *Phys. Rev. B* **92**, 195409 (2015).
- [32] P. Kirton and J. Keeling, Nonequilibrium Model of Photon Condensation, *Phys. Rev. Lett.* **111**, 100404 (2013).
- [33] In any real experiment, there will be a slight anisotropy to break the degeneracy, resulting in a definite set of photon modes. In the isotropic case, however, any orthonormal set of linear combinations of modes within a degenerate subspace is an equally valid choice, and choosing any particular set would be arbitrary. Therefore, to avoid any ambiguity, we choose the slightly anisotropic case in our simulations.
- [34] This quantity is proportional to the usual definition of the gain as the measure of the difference between stimulated emission and absorption. For simplicity, we refer to it as the gain throughout the paper.
- [35] D. McCumber, Einstein relations connecting broadband emission and absorption spectra, *Phys. Rev.* **136**, A954 (1964).
- [36] P. Moroshkin, L. Weller, A. Saß, J. Klaers, and M. Weitz, Kennard-Stepanov Relation Connecting Absorption and Emission Spectra in an Atomic Gas, *Phys. Rev. Lett.* **113**, 063002 (2014).
- [37] The pump can also be modeled as a very wide Gaussian beam, to more accurately correspond to the experiment. This introduces only minor quantitative changes into the work presented here, without affecting any of the qualitative results.
- [38] R. A. Nyman, Absorption and Fluorescence spectra of Rhodamine 6G (Zenodo, 2017), <https://doi.org/10.5281/zenodo.569817>.
- [39] D. Vorberg, W. Wustmann, R. Ketzmerick, and A. Eckardt, Generalized Bose-Einstein Condensation into Multiple States in Driven-Dissipative Systems, *Phys. Rev. Lett.* **111**, 240405 (2013).
- [40] D. Vorberg, W. Wustmann, H. Schomerus, R. Ketzmerick, and A. Eckardt, Nonequilibrium steady states of ideal bosonic and fermionic quantum gases, *Phys. Rev. E* **92**, 062119 (2015).
- [41] A. E. Siegman, *Lasers* (University Science Books, Mill Valley, CA, 1986).
- [42] J. Klaers, J. Schmitt, T. Damm, F. Vewinger, and M. Weitz, Statistical Physics of Bose-Einstein-Condensed Light in a Dye Microcavity, *Phys. Rev. Lett.* **108**, 160403 (2012).
- [43] R. L. Fork and M. A. Pollack, Mode competition and collision effects in gaseous optical masers, *Phys. Rev.* **139**, A1408 (1965).
- [44] P. W. Smith and R. Hänsch, Cross-Relaxation Effects in the Saturation of the 6328-Å Neon-Laser Line, *Phys. Rev. Lett.* **26**, 740 (1971).
- [45] K. Otsuka, P. Mandel, S. Bielawski, D. Derozier, and P. Glorieux, Alternate time scale in multimode lasers, *Phys. Rev. A* **46**, 1692 (1992).
- [46] Alternatively, we could consider (a), (b), and (c) to correspond to different cavities, which have the same photon loss rate  $\kappa$  at the given cutoff frequencies.